ATMOSPHERIC SCIENCE

Projected increase in the frequency of extremely active Atlantic hurricane seasons

Hosmay Lopez[1]*, Sang-Ki Lee[1], Robert West[1,2], Dongmin Kim[1,2], Gregory R. Foltz[1], Ghassan J. Alaka Jr.[1], Hiroyuki Murakami[3]

Future changes to the year-to-year swings between active and inactive North Atlantic tropical cyclone (TC) seasons have received little attention, yet may have great societal implications in areas prone to hurricane landfalls. This work investigates past and future changes in North Atlantic TC activity, focusing on interannual variability and evaluating the contributions from anthropogenic forcing. We show that interannual variability of Atlantic TC activity has already increased, evidenced by an increase in the occurrence of both extremely active and inactive TC seasons. TC-resolving general circulation models project a 36% increase in the variance of North Atlantic TC activity, measured by accumulated cyclone energy, by the middle of the 21st century. These changes are the result of increased variability in vertical wind shear and atmospheric stability, in response to enhanced Pacific-to-Atlantic interbasin sea surface temperature variations. Robust anthropogenic-forced intensification in the variability of Atlantic TC activity will continue in the future, with important implications for emergency planning and societal preparedness.

INTRODUCTION

Tropical cyclones (TCs) are among the most deadly and costly natural disasters that affect the US [National Oceanic and Atmospheric Administration (NOAA)/National Weather Service Natural Hazard Statistics, 2021) and many other countries each year. Hence, the scientific community has placed great efforts not only in improving their predictions, but also in understanding how global and regional TC activity have changed and will continue to change under anthropogenic forcing. For example, while there is a projected 13% decrease in global TC frequency, TCs are projected to become around 5% more intense in most global climate models (*1*–*5*), indicating that greenhouse warming will shift global TCs toward stronger storms (*6*). Recent studies argue that changes in TC activity are detectable in the present day (*7*, *8*), with external anthropogenic effects having already emerged over natural variability (*9*). However, separating natural and anthropogenic modulations remains a challenge (*7*).

While global TC activity have shown a decreasing trend (*10*), the North Atlantic basin has experienced a pronounced increase in the number of TCs and accumulated cyclone energy (ACE) over the past 50 years. Previous studies reported that these increases in the North Atlantic could be associated with changes in anthropogenic aerosols (*11*). In addition, observational trends in TC activity, specifically TC intensity, could also be influenced by artificial trends owing to the evolution of observing systems (*12*–*14*). For example, there has been an increase in the frequency of short-lived storms (<2 days) since around the year 2000, a fact that has been shown to be artificially created by the inhomogeneity in the observing systems and improvements in observational capabilities (*15*, *16*). However, these short-duration storms have little to no impact on seasonal ACE; thus, ACE records should be relatively reliable from 1970 onward, thanks to the combination of Dvorak satellite estimates and aircraft reconnaissance flights. In addition, it is difficult to distinguish between trends driven by external forcing [e.g., anthropogenic climate change (ACC)] and those driven by internal climate variability such as the Atlantic multidecadal oscillation (AMO) (*17*, *18*) or the Interdecadal Pacific Oscillation (*19*–*22*). This is due to the fact that the year-to-year TC variability is much larger than the observed and/or projected future trends. That is, the projected changes in TC climatology are much smaller than the observed internal variability of seasonal TC activity: A 2°C global mean temperature increase results in a North Atlantic TC frequency decrease of 15%, or about 2 TCs per year (*23*), while the year-to-year variability in the number of named storms is much higher (e.g., 28 named storms in 2005, 8 in 2014, and 30 in 2020), corresponding to a SD of 5 TCs. Despite these large year-to-year fluctuations, future changes in TC variance are rarely investigated in detail, resulting in considerable uncertainty in climate projections of TC activity and landfalls (*23*).

In the North Atlantic basin, TCs frequently develop during June-November between 10°N-20°N and 60°W-20°W, an area known as the main development region (MDR) (*24*, *25*). While the genesis of a specific TC is strongly dependent on short-term atmospheric variability, e.g., African easterly waves (*26*) and intraseasonal variability, e.g., convectively coupled Kelvin waves and the Madden-Julian oscillation (*27*, *28*), interannual and longer-term modulations of TC frequency are influenced by slowly varying local and remote ocean-atmosphere interactions. For example, on interannual timescales, the Atlantic warm pool and Atlantic Meridional Mode modulate sea surface temperature (SST) variability in the tropical North Atlantic and Intra-Americas Sea via anomalous surface heat flux (*29*–*31*) and wind-evaporation-SST feedback (*32*). Therefore, these SST modes are highly correlated with Atlantic TC activity on interannual timescales (*33*, *34*).

Forcing from remote regions is also an important modulator of Atlantic TC activity (*35*–*39*). For example, tropical Pacific SST anomalies (SSTAs) linked to the El Niño–Southern Oscillation (ENSO) are a major driver of interannual TC activity and are therefore often used as a seasonal predictor for TC activity in the Atlantic basin. Specifically, the positive phase of ENSO (El Niño) warms the tropical troposphere (*40*), reducing atmospheric convection and increasing

[1]Atlantic Oceanographic and Meteorological Laboratory, NOAA, Miami, FL, USA. [2]Cooperative Institute for Marine and Atmospheric Studies, University of Miami, Miami, FL, USA. [3]Geophysical Fluid Dynamics Laboratory, NOAA, Princeton, NJ, USA. *Corresponding author. Email: hosmay.lopez@noaa.gov

vertical wind shear over the Caribbean and Gulf of Mexico and consequently reducing Atlantic TC activity (*41*–*46*). Thus, the interbasin SST difference between the tropical North Atlantic (MDR) and tropical Pacific has been identified to modulate seasonal Atlantic TC activity (*47*–*51*) and TC maximum potential intensity (*49*, *52*) in the Atlantic basin.

Given that seasonal TC activity in the North Atlantic is largely modulated by the difference in SSTAs between tropical Atlantic and Pacific basins (*47*–*54*), a projected increase in the interannual variability of ENSO (*55*) and tropical North Atlantic SST (*56*) suggests an increase in the interannual variability of the future interbasin SST difference and hence North Atlantic TC activity. However, future projections of ENSO and its remote effects are still uncertain due to model biases (*57*, *58*). A recent work (*59*) used idealized SST-forced model experiments to investigate how extremes in seasonal Atlantic TC activity may change due to the joint effects of ENSO and the Atlantic Meridional Mode and found that extremely active seasons becomes more common under anthropogenic effects, with greater TC number and a shift to stronger TCs. While these results are based on a single SST-forced model, without air-sea feedbacks, it highlights the importance of considering changes in the mean and interannual climate variability influencing TC activity. The primary objective of this work is to determine whether there have been changes in interannual variations of TC activity and if so, whether they will continue into the future. These questions are motivated by two premises: (i) Future changes in the variance of TC activity may have a greater societal impact than the change in the mean and (ii) interannual variability of dominant climate drivers (e.g., ENSO and tropical Atlantic SST) that modulates North Atlantic TC activity is projected to increase. Thus, we hypothesize that interannual variability of North Atlantic TC activity will intensify as a result of the enhanced interbasin SST variations in the future. Consequently, extremely active seasons (e.g., 2005 and 2020) and inactive seasons (e.g., 2014) will become more common with remarkable socioeconomic implications. For the remainder of this paper, TC activity refers exclusively to that of the North Atlantic basin.

RESULTS

Observed changes in the mean and interannual variability

The observed changes in TC activity in the North Atlantic basin are analyzed on the basis of the number of TCs and ACE, excluding the short-lived storms (<2 days; see Materials and Methods) to avoid artificial trends due to changes in the observing system. While TC observations for the Atlantic date back to the 1800s, the 1970 to 2023 analysis period is chosen here to avoid missing TCs due to observational limitations prior to the satellite era, before 1966 (*12*, *60*). Consistent with earlier studies (*9*, *61*), both ACE and the number of TCs have increased at a rate of $16.9 \pm 9.1 \times 10^4$ kt^2 per decade for the former (Fig. 1A) and 1.36 ± 0.58 per decade for the latter (Fig. 1B). Since ACE is an integration of multiple factors, e.g., TC number, lifetime, and intensity, it is worth investigating their relative contribution to the observed mean and variance changes of ACE (see the Supplementary Materials). About 83% of the trend in seasonal ACE is explained by a trend in TC number–induced ACE ($14.03 \pm 4.96 \times 10^4$ kt^2 per decade), whereas only 6% of the trend in seasonal ACE is explained by a trend in lifetime-induced ($0.99 \pm 3.56 \times 10^4$ kt^2 per decade) and 11% is explained by intensity-induced ($1.94 \pm 3.63 \times 10^4$ kt^2 per decade) ACE. That is, most of the observed trends in ACE can be attributed to an increase in TC number. In contrast, observed trends in lifetime and intensity are not statistically significant (table S1 and fig. S1).

The 20-year running average standard deviation also shows substantial increases in the interannual variability of ACE and the number of TCs. Specifically, a statistically significant upward trend is found in the interannual standard deviation of both ACE ($3.80 \pm 0.84 \times 10^4$ kt^2 per decade; Fig. 1C) and the number of TCs (0.40 ± 0.03 per decade; Fig. 1D). While the ACE and TC number trends are positive for the observed period, it is worth noting that the behavior is more of a regime change, with enhanced interannual variability in the later period, a feature that has been documented as a switch between the inactive and active era, which coincided with a shift from a negative to a positive phase of the AMO (*17*, *18*), as well as a reduction in anthropogenic aerosols (*9*, *11*). A variance ratio analysis for the relevant SST indices that are known to influence ACE shows that the variability over the Niño3 region has increased by about 12% since 1995, whereas the SST variance over the MDR has increased by about 27% in the same period, all consistent with the increase in ACE and TC number variability observed since 1995.

These results pose the question: Is the recent increase in ACE and the number of TCs due to a mean increase in TC activity, i.e., an increase in the median with little change in the tails (Fig. 1, A and B), and/or due to an increase in the observed interannual variability of TC activity, i.e., more extreme seasons (Fig. 1, C and D)? This question is tackled by splitting the observed period into early and recent periods, ranging from 1970 to 1994 and 1995 to 2023, respectively. This separation is motivated by the observed upward trends in TC activity and interannual variability. It is found that the variance ratio for the later versus the earlier period ranges from 2.30 to 2.75 for ACE and 2.60 to 2.81 for the TC number, where the ranges are obtained by testing the robustness of the cutoff point by shifting the computation by 5 years back and forward centered at the two periods. This is done given that the shift in TC activity could be influenced by natural decadal variability and the choice of the cutoff point (*17*–*21*). As shown, the results are robust and independent of the choice of time window, which are showing a significant increase in variance at 95th percentile based on an *F* test.

A probability density functions (PDFs) of observed ACE and TC number are modeled by a stochastically generated skewed (SGS) distribution (*62*, *63*) (see Materials and Methods, table S2, and fig. S2 for details on the choice of distribution and goodness-of-fit analysis). Figure 1 (E and F) shows the observed SGS distributions for ACE and TC number, respectively. Four different parameter configurations are used to construct the PDFs, using statistical moments derived from: (i) the early period, (ii) early period plus observed mean changes only, (iii) early period plus observed variance changes only, and (iv) recent period, which includes mean plus variance changes. Note that the observed increases in ACE and TC number are explained by increases in the mean, whereas the broadening of the PDF due to increased interannual variability is responsible for more extreme seasons (Fig. 1, E and F). While the mean increase is large and statistically significant, the increase in interannual variability also appears to contribute to the occurrence of extreme TC activity seasons since 1995, such as the extremely active 2005 and inactive 2014 seasons. The return periods for such extreme seasons are computed directly from these SGS PDFs and are shown in table S3. Extremely active seasons, such as the 2005 season with greater than 18 named storms are rarely expected to occur in the early period

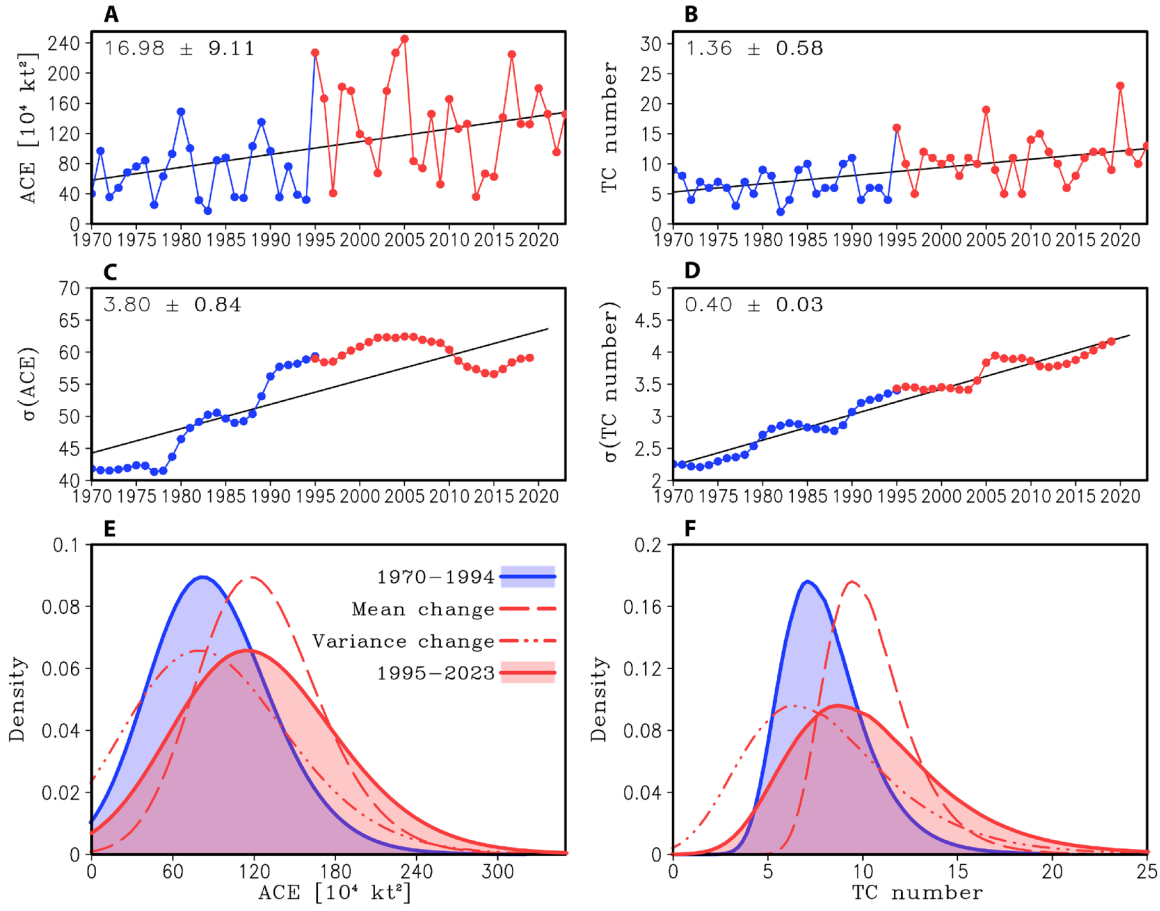

Fig. 1. Observed time series of Atlantic TC activity. (**A**) Accumulated cyclone energy (ACE; 10^4 kt^2) and (**B**) number of TC from 1970 to 2023. The black line corresponds to the linear trend with value shown in the top-left depicting the decadal trend plus/minus its 95% confidence interval. (**C**) Twenty-year running averaged SD of ACE centered at the year labeled in the abscissa. For example, the SD around the year 2000 corresponds to the period of 1990 to 2009. The early period (i.e., 1970–1994) and recent period (i.e., 1995–2023) are denoted by blue and red lines, respectively. (**D**) Same as (C) but for number of TCs. (**E**) Stochastically generated skewed (SGS) probability density function (PDF) of ACE for different parameter sets (see Materials and Methods) obtained from: early period (solid blue), early period plus accounting for mean change only (dash-red), early period plus accounting for variance change only (dot-dot-dash red), and recent period (solid-red). (**F**) is similar to (E) but for TC numbers.

(1970–1994), with a return period of greater than 1000 years. However, such extreme seasons become increasingly common when accounting for mean changes (every 168 ± 31 years), variance changes (every 41 ± 5 years), and both mean and variance changes (every 21 ± 2 years). Similar results are obtained for the return period of the extreme ACE observed in 2005 (245×10^4 kt^2; table S3). Note that the increase in variance is responsible for a larger reduction in the return period of high impact TC seasons like 2005 (i.e., they happen more frequently) than the increase in the mean.

Regarding extremely quiescent seasons like 2014, which had only eight named storms (6 TCs with greater than 2-day lifetime), the return period during 1970 to 1994 was about 20 ± 8 years. If only the mean changes are accounted for, the return period increases to more than 1000 years. However, such an event becomes more common, occurring every 4 ± 1 years, if only the variance changes are considered, and less common, occurring every 14 ± 4 years, if both the mean and variance changes are accounted for (e.g., the recent period). Similarly, the return period of low ACE values (e.g., 66.7×10^4 kt^2 as in 2014) is shortened (i.e., more common) when accounting for variance changes. In summary, changes in interannual variability have played a dominant role in determining the occurrence of the extremely active and extremely inactive TC seasons observed since 1995. Hence, increases in the mean and interannual variability have had a compounding (opposing) effect on the occurrence of active (inactive) TC seasons.

Future projections—Direct detection from HighResMIP

Is the observed increase in interannual variability, and thus occurrence of extremely active and inactive TC seasons, projected to continue due to anthropogenic effects? To address this question, here, we examine future projections of TC activity based on direct detection of TCs from uncoupled and fully coupled models of the High-Resolution Model Intercomparison Project [HighResMIP, (*64*)]. The atmospheric components of the selected models have resolutions of approximately 50 km or higher, allowing for explicit simulation of hurricanes (*65*). These model runs followed the Shared Socioeconomic Pathways (SSP5.8.5) emission protocol and were integrated from 1950 to 2050. See Materials and Methods and table S4 for model details. TCs are detected by two fundamentally different tracking algorithms (see Materials and Methods).

Before evaluating future changes in SST variability, we verify if the observed relationship between ACE and SST is reproduced in the HighResMIP models for the historical period. Note that while both coupled and uncoupled models are able to reproduce the observed interbasin SST contrast (cold Pacific–warm Atlantic), the uncoupled simulations perform better, especially in depicting the amplitude of the SST signal (fig. S3). The coupled (uncoupled) simulations show a weaker (stronger) ACE-SST relationship relative to observations, most notably in the ACE-tropical Pacific SST relationship. While the coupled models tend to have larger biases than their uncoupled counterparts (*65*–*67*), the uncoupled models tend to overestimate the ACE-SST relationship due to the lack of negative feedback from TC interactions with the ocean (*64*). However, the Atlantic ACE-SST correlation is well represented in the ensemble mean. In addition, the spatial correlation is fairly high for most models ($r > 0.6$), and the root mean square errors are small and unsaturated for all ensembles, thus adding confidence that the HighResMIP represents very well the ACE-SST relationship.

Most HighResMIP models show the correct sign of increasing variances in ACE and TC number (fig. S4) but tend to underestimate the observed trends in interannual variability for the 1970 to 2023 period (Fig. 1, C and D). Analysis of projected changes in interannual variability of ACE and TC number for these HighResMIP model runs is performed for two separate periods: 1970 to 2019 (hereafter historical period) and 2020 to 2049 (hereafter future period). Figure 2 shows the projected changes in interannual variability of ACE (Fig. 2A) and TC number (Fig. 2B) as measured by the variance ratio of future versus historical periods. The analysis is further divided by those models that depict the "correct" versus "incorrect" observed positive variability trend (fig. S4). Note that most models show a notable increase in the variance of ACE. Since the variance ratio is computed for each individual model, it is an unbiased estimate of projected changes in future activity relative to the historical period. The majority of the models show an increase in future variability relative to historical period. Specifically, the multimodel mean consensus is a 36 ± 17% increase in ACE variability, which is significant at the 95% confidence level based on a bootstrapping technique (see Materials and Methods). Results for TC number are similar, with the majority of the models depicting an increase in interannual variability: The ensemble mean increases by 19 ± 11%, also significant at the 95% confidence level. In addition, the models depicting the correct sign of the observed trend (red marks in Fig. 2) show a further increase in the future to historical variance ratio of 52 ± 18% for ACE and 38 ± 14% for TC number, whereas those models that show the incorrect trends (blue marks in Fig. 2) show a slight reduction in future variance that is not statistically significant. It is worth noting that the increase in variance is considerably larger than the projected mean changes for ACE and TC number (table S5).

The analysis of decomposing ACE into its three constituents (TC number, lifetime, and intensity) is repeated for the HighResMIP. In all, while all three components contribute to a projected increase in ACE variance, TC number is the primary reason for the projected changes in interannual variability of ACE (fig. S5). Separating the variance ratio analysis by tracking algorithm (fig. S6) shows that TC number is more dependent on the algorithm used than ACE, driven by discrepancies in the number of TCs detected by each tracking algorithm, i.e., more weak storms detected in the TRACK versus the TempestExtremes (*68*). It is also known that ACE is a more robust measure of TC interannual variability than TC number (*69*, *70*). Nevertheless, overall, both detection algorithms consistently show future increases in interannual variability of ACE and TC number (fig. S6).

The HighResMIP contains both coupled and uncoupled (i.e., SST-prescribed) runs (*64*). Each has advantages and disadvantages. While the coupled runs better represent important air-sea interactions relevant to TC activity, they tend to produce weaker storms due to negative feedback from TC interactions with the ocean (*64*) and generally have inherently larger biases than the prescribed runs. On the other hand, the uncoupled runs in the HighResMIP protocol do not include changes in interannual variability of SSTs for future projections. This is a noteworthy caveat that substantially diminishes the utility of the uncoupled simulations for the purpose of this study because projected changes in ENSO and MDR SST variability are not accounted for, and only the mean SST changes from Coupled Model Intercomparison Project version 6 (CMIP6) future projections are prescribed (*64*). However, we choose to analyze the uncoupled runs as they usually contain smaller biases than their coupled counterparts (*64*, *66*, *67*) and to add ensemble size for increased degrees of freedom. The uncoupled runs also provide an estimate of the TC variance changes unrelated to the SST interannual variability, such as mean SST changes and internal atmospheric mean and variance (e.g., potential intensity modulations).

Thus, it is worth separating the analysis into coupled and prescribed SST runs. Both sets show an increase in variability, although the uncoupled runs have larger variance increase of ACE than the coupled runs (fig. S6). More specifically, in the prescribed runs, an ENSO event of similar amplitude would produce a stronger teleconnection to the MDR in the future compared to the historical period since the tropical mean state is much more convective in the future in CMIP6, i.e., El Niño–like mean state (*55*, *71*). We also quantify the percent of models that shows an increase, statistically significant increase, decrease, and statistically significant decrease in interannual variability for the projected period (2020–2049) relative to the observed period (1970–2019) for ACE and TC number (table S6). Substantially more models suggest a projected variance increase independently of coupling, although this is more robust in the uncoupled runs. With that said, it is not possible to attribute specific causes of the discrepancies between coupled and uncoupled runs (e.g., coupling biases and mean state changes), and their contribution to internal atmospheric dynamics relevant to TC variations, without performing dedicated model experiments. It is worth noting that the coupled models underrepresent the observed ACE-SST relationship, most notably the tropical Pacific SSTs, potentially reducing the role of projected ENSO variance increase (*55*) and its Atlantic TC modulations (fig. S3). For the Atlantic basin as a whole, changes in the interannual variability of TC activity are greater than changes in mean activity, arguing for more extreme swings between active and inactive hurricane seasons and highlighting the importance of variability changes in future projections.

While the discussion in this work is centered on changes in interannual variability of ACE, it is worth assessing the spatial structure of TC activity pertaining to both mean and interannual variability. Note that the HighResMIP is able to reproduce the observed spatial distribution of TC activity (see Materials and Methods and figs. S3, S7, and S8 for further discussion on strengths and weaknesses of these models). Figure 3 describes the future projected changes in mean TC activity and its interannual variability relative to the historical period

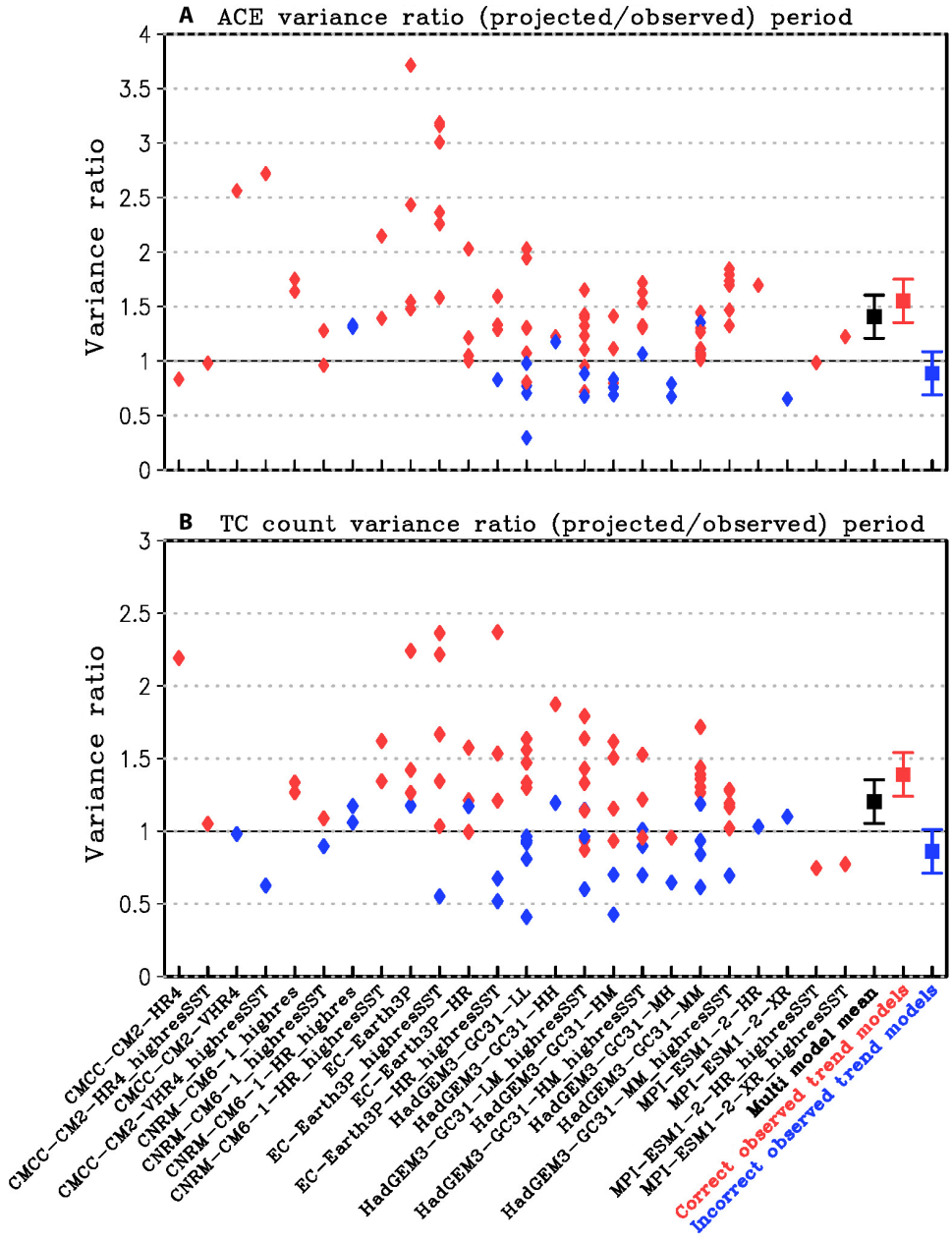

Fig. 2. Direct simulation of Atlantic TC activity changes. Changes in interannual variability as measured by the projected (2020–2049) to observed (1970–2019) period variance ratio from June to November for (**A**) ACE and (**B**) TC number from 24 models from the High-Resolution Model Intercomparison Project (HighResMIP). The analysis is separated into models that accurately depict the observed trends (red) and those that depict the incorrect observed trend (blue). The ensemble mean for all models is shown at the far right in black along with confidence intervals at a 95% level based on a bootstrapping technique (see Materials and Methods). The multimodel mean for those models depicting the correct (incorrect) historical trend is also shown in the far right in red (blue).

from HighResMIP. Note the dipole structure of the projected changes in mean TC track density (Fig. 3A) and genesis location (Fig. 3C), with increased activity over the Atlantic and a reduction in activity in the Caribbean Sea. The dipole structure shown in Fig. 3A is remarkably similar to the observed storm-track density changes, which also indicate a decrease (increase) in track density over the western (central and eastern) Atlantic basin (*12*, *72*). While some of the spatially inhomogeneous observed trends have been attributed to observing system changes, e.g., increased observations in the central and eastern Atlantic (*15*), the fact that future projections from HighResMIP (Fig. 3, A and C) show a similar trend indicates that anthropogenic effects are also playing a major role in generating the unequal spatial structure of the trends in Atlantic TC activity. This agreement between model and observations is remarkable given that historical trends in the tropical SST show a La Niña–like pattern, whereas most models show an El Niño–like trend (*73*). However, other external forcings, such as the diminishing effect of anthropogenic aerosols and volcanic activity, could also play a fundamental role in the

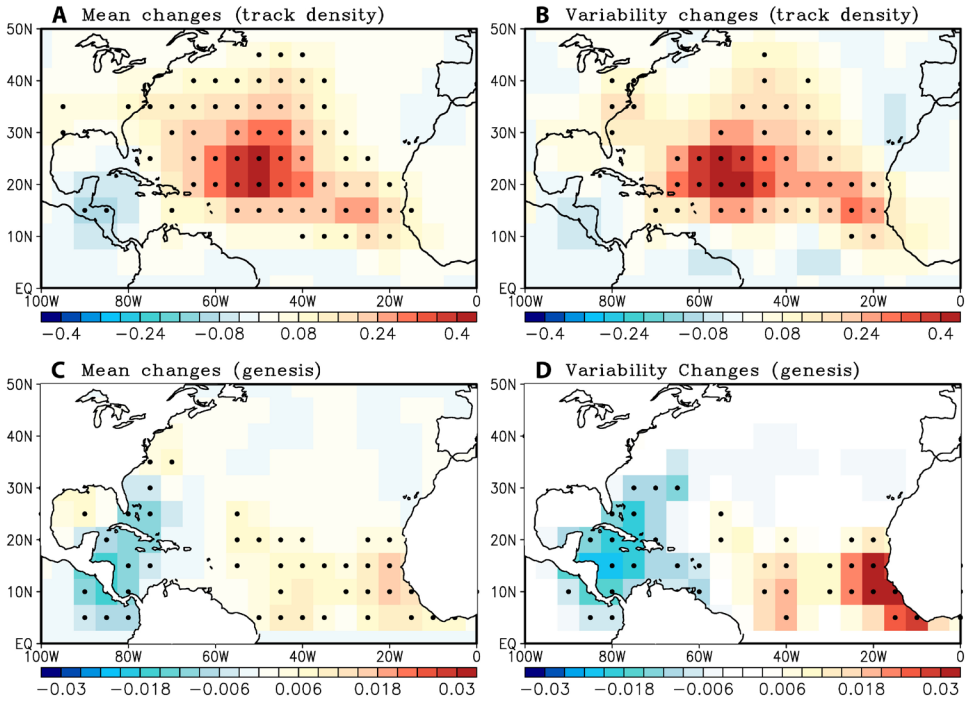

Fig. 3. Spatial distribution of projected changes in TC activity. Changes in track density (top) and genesis location (bottom) per 5° latitude-longitude box per year from the HighResMIP simulations measured by the differences between the projected (2020–2049) minus the observed (1970–2019) period. (**A**) Mean track density changes and (**B**) interannual track density variability changes. Similarly, (**C** and **D**) show mean genesis and interannual genesis variability. Stipples indicate statistical significance at the 95% confidence level based on a bootstrapping technique (see Materials and Methods).

observed TC activity changes (*9*). This dipole structure of trends is consistent with some previous studies, which attribute the eastward shift to changes in genesis location and background flow (*74*–*76*). In contrast, other studies have suggested an overall decrease in future track density (*77*). The seemingly conflicting results could be model dependent and/or tracking method dependent, further motivating the use of multimodel ensembles and different detection and tracking algorithms.

In contrast to the inhomogeneous changes in mean TC activity, projected changes in the interannual variability of TC track density show a more consistent increase throughout the Atlantic basin (Fig. 3B), with a notable increase from Cabo Verde to the southeast coast of the U.S. Changes in the variance of TC genesis (Fig. 3D) show a spatially inhomogeneous pattern, with a projected increase (decrease) in variability over the eastern Atlantic and MDR (Caribbean). This suggests that increased variability of TC genesis over the MDR leads to increased TC track density north of the MDR. The MDR is a net exporter of ACE and much of the ACE that originates in the MDR ends north of it (Fig. 3, A and B). A recent study found that ENSO tends to modulate TC genesis and track density predominantly in the southern Gulf of Mexico and Caribbean Sea with little to no impact in the rest of the basin (*78*). Thus, the reduced TC activity over the Caribbean Sea shown in Fig. 3 is consistent with a projected El Niño–like mean state in the Pacific (*55*, *79*–*83*), which should decrease TC activity in the Caribbean Sea (*78*).

Projected changes in large scale drivers—CMIP6

Seasonal Atlantic TC activity (i.e., ACE) is largely modulated by the SST difference between the tropical Atlantic and the tropical Pacific (*49*–*54*). This is illustrated in fig. S3, which shows the correlation between seasonal averaged ACE for the Atlantic basin and SSTAs over each grid-point highlighting the well-known warm MDR–cold tropical Pacific pattern that enhances TC activity in the Atlantic basin (*53*, *54*). Thus, an important question is if the current and projected future increases in TC variance (Figs. 1 to 3) are driven by enhanced interbasin SST variability and/or large-scale environment factors known to modulate TC activity, like vertical wind shear and mid-level atmospheric stability (*84*). Thus, we assess future changes in SST variability in CMIP6 between the present climate and future projections using the Shared Socio-economic Pathway SSP5-8.5 emissions scenario (list of models in table S7). Before looking at future changes, we computed the variance ratio for recent period (1995–2023) relative to the earlier period (1970–1994) for SSTs, vertical wind shear, and atmospheric stability (i.e., lifted index) averaged over the MDR from observations and CMIP6 simulations (Fig. 4). Note that all three environmental parameters show a variance increase. For example, 12 of 15 CMIP6 models show an increase in the vertical wind shear variance (Fig. 4A) and atmospheric stability variance (Fig. 4B) and 11 of 15 models suggest an increase in SST variance (Fig. 4C) and denoted by a variance ratio that is greater than one.

Regarding future changes in large-scale environmental factors, a recent study argues that El Niño events are projected to develop earlier and more strongly during boreal summer and fall, with enhanced overall interannual variability in CMIP6 (*55*). Tropical North Atlantic SST variability is also projected to increase (*56*), driven by an intensification of the ENSO-forced Pacific-North American pattern and associated surface heat flux anomalies. Future changes in large-scale

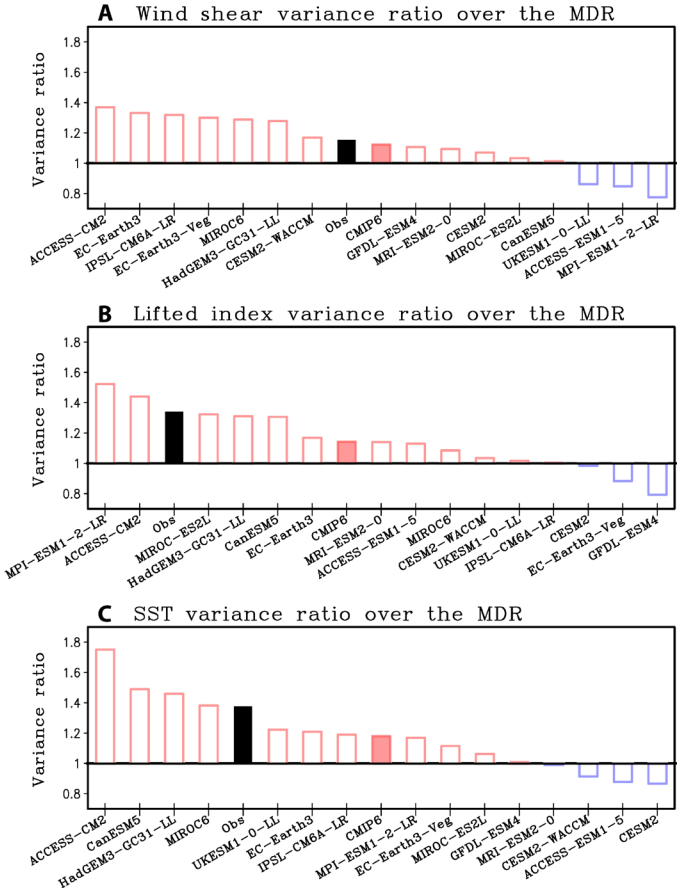

Fig. 4. Observed and modeled changes in interannual variability. Variance ratio of (**A**) 200 to 850 hPa vertical wind shear, (**B**) 500 hPa lifted index, and (**C**) sea surface temperature (SST) averaged over the Atlantic main development region (MDR, 10°N-20°N and 60°W-20°W). Positive (negative) values indicate increase (decrease) interannual variability for the recent period (1995–2023) relative to the earlier period (1970–1994). The ensemble mean of the Coupled Model Intercomparison Project version 6 (CMIP6) models is shown by a red bar. The observed variance ratio is also shown by a black box for comparison.

atmospheric variability responsible for TC activity are described in Fig. 5 by the variance ratio, i.e., 21C versus 20C interannual variance, for (A) 20- to 850-hPa vertical wind shear, (B) atmospheric stability as measured by the 500 hPa lifted index, and (C) SST. There are projected increases in interannual variability in all three variables over the Atlantic MDR. The increases are consistent with the projected increases in variance for ACE and TC number (Fig. 2). Note that 13 of 15 CMIP6 models show a variance increase of vertical wind shear and atmospheric stability and all models suggest a variance increase in SSTs (fig. S9), suggesting a future enhancement of interannual variability of Atlantic wind shear, atmospheric stability, and SST. In addition to changes in interannual variability, the projected increase in the mean surface temperature would translate into a larger atmospheric response to interbasin SST variations (*71*).

Attribution analysis of extreme TC activity

Attribution analysis of TC activity is carried out here using the projected changes in direct TC representation from HighResMIP models. This analysis is further validated with an interbasin SST proxy for ACE (*51*). This SST proxy is derived from the linear regression between observed ACE and the interbasin SSTA difference (i.e., Atlantic MDR minus Niño 3 SSTAs) chosen for the CMIP6 simulations because the coarse resolutions of these models do not allow accurate representations of TC development and evolution (*85*). It is worth noting that the interbasin SST proxy for ACE used here has a correlation of 0.67 with the observed Atlantic ACE for the historical period of 1970 to 2023, and is conceptually very similar to the traditional Atlantic MDR minus tropical SSTAs (*83*, *86*). However, the relationship between global SST and ACE does not necessarily need to be stationary under external forcing. For example, the projected shift to more intense storms (*6*) have been attributed to not just changes in the SSTs but to changes in the upper troposphere temperature (*87*–*89*). In addition, the recent downward trend in TC outflow temperature associated with a cooler tropical tropospheric layer is a major contributor to the observed increase in potential intensity of TCs (*87*, *88*). With that said, the SST-ACE relationship is

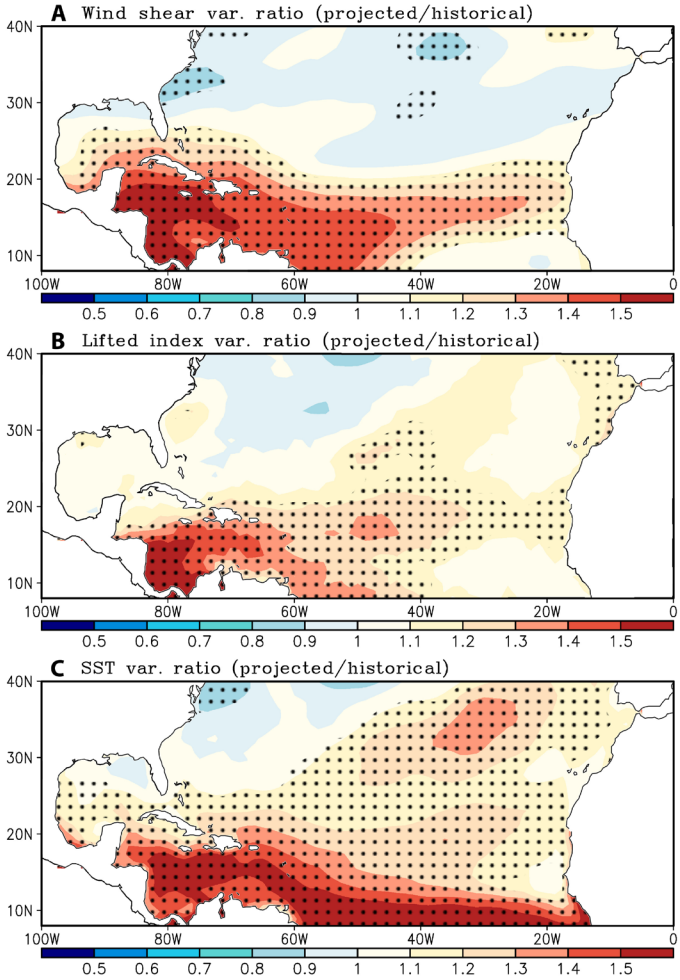

Fig. 5. Interannual variability changes of selected large-scale TC environment fields. The projected to historical period variance ratio from June to November for (**A**) 200 to 850 hPa vertical wind shear, (**B**) 500 hPa lifted index, and (**C**) SST. Positive (negative) values indicate projected increase (decrease) interannual variability. Stipples indicate statistical significance at the 95% confidence level based on a bootstrapping technique (see Materials and Methods).

still present in the future projections period (fig. S10, 2020–2049), so we choose the interbasin SST proxy for ACE to investigate future projection from the CMIP6 simulations.

The definition of the time of emergence (ToE) involves defining a signal-to-noise ratio. Here, we take the external forcing signal as the ensemble mean (i.e., forced component) versus the ensemble spread (i.e., natural variability) in fully coupled CMIP6 simulations. The influence of anthropogenic forcing on the near-future distribution of extreme TC activity, including the tercile frequency of active, neutral, and inactive Atlantic TC seasons, is assessed in Fig. 6. The definition of what constitutes an active season is based on NOAA/Climate Prediction Center seasonal ACE thresholds (i.e., below-, near-, and above-average activity). Figure 6A shows the time series of likelihood of seasonal ACE derived from the interbasin SST proxy from CMIP6 for each tercile category. Since the threshold for each tercile is drawn from the 1920 to 2000 PDF, the expected value for each tercile is one-thirds for the 20th century. To assess changes in the likelihood of each tercile (e.g., nonstationarity), the thresholds are fixed at the 20th century levels throughout the 1920 to 2100 period. Note that there are expected increases in the numbers of years with above- and below-normal TC activity for the Atlantic basin, together with a reduction in the number of near-normal activity seasons. This suggests a broadening of the spectrum distribution of TC activity. Figure 6A can also be used to estimate the ToE of anthropogenic signals with regard to TC activity. Note that by the 2020s, the probability of near-normal seasons is notably lower than the expected 33% tercile probability, increasing the probabilities of above- and below-normal seasons. This suggests that anthropogenic forcing is driving enhanced interannual variability in TC activity. One limitation of using the ensemble mean of CMIP6 models to define the external forcing is that climate models tend to have common biases due to similar parametrization (*90*); thus, the ensemble mean could still contain some portion of model biases. In addition, multidecadal climate variability has been shown to consists of a superposition of low-frequency signals, with both natural and external sources (*91*, *92*). For example, volcanic and anthropogenic aerosols may have contributed to the recent AMO cycles via a reduction (increase) of surface solar radiation and thus cooling (warming) of SSTs (*93*, *94*). Thus, separating the natural and all external components requires dedicated single-forcing experiments, which is beyond the scope of this work.

The increase in active and inactive seasons and reduction of near-normal seasons are further corroborated by direct simulations of TCs from HighResMIP (Fig. 6B). For this analysis, the tercile thresholds are determined from standardized anomalies; $z = (x - \mu)/\sigma$, where x is the ACE value for each model, and μ and σ are the historical period (1970–2019) mean and SD of ACE for the specific model. This approach facilitates comparison among models with distinct TC representations (fig. S6). For each of the 87 ensembles (table S4), the instances for above-, near-, and below-normal terciles are counted for the future period (2020–2049) using the historical period thresholds. A PDF is then computed using all 87 ensembles and shown in Fig. 6B. The probabilities of above-, near-, and below-normal TC seasons are: 38 ± 1.8%, 26.7 ± 2.0%, and 35.4 ± 1.8%, all significantly different than the expected 33.3%. The enhanced above- and below-normal terciles and reduced near-normal tercile are consistent with the results based on the interbasin SST proxy (Fig. 6A).

Projected changes in the PDF of seasonal TC activity have large socioeconomic implications, especially if the high-impact (i.e., above-normal) tercile is projected to increase in frequency. Thus, it is worth investigating the role of anthropogenic effects on high-impact extreme seasons such as 2005. Note that this is not an attempt to attribute the very active seasons of 2005 to natural versus anthropogenic causes, but rather to assess the likelihood that an extreme season with large ACE values was anthropogenically caused. That is, without anthropogenic forcing, the event would not have occurred. Hence, we rely on causal counterfactual theory (*95*, *96*) applied to present and future simulations of TC activity

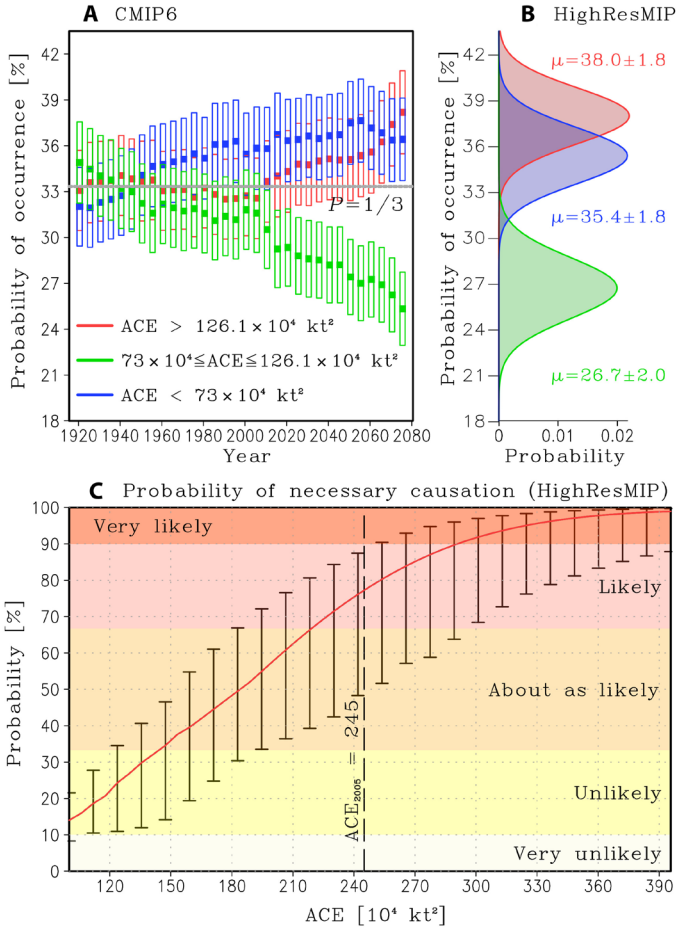

Fig. 6. Attribution analysis of future changes in Atlantic TC activity. (**A**) Temporal evolution of a 30-year running average number of above-normal (red), near-normal (green), and below-normal (blue) TC seasons based on interbasin SST-derived ACE from the CMIP6 simulations. The boxes denote the ensemble spread. The light-colored horizontal line denotes the expected equal (one-thirds) probability for terciles. The year labels on the abscissa correspond to the central year of the 30-year window. For example, the year 2030 indicates the period spanning 2016 to 2045. ACE thresholds denoting above-, near-, and below-normal TC activity follow those of the NOAA/Climate Prediction Center and are noted in the legend. (**B**) PDF of probabilities of above (red), neutral (green), and below normal (blue) Atlantic hurricane activity derived from HighResMIP simulated TC activity for the 21st century (2020–2049) period. The mean (μ) plus/minus the 95% confidence intervals based on a bootstrapping technique are also shown (see Materials and Methods). (**C**) Probability of necessary causation (PN) shown by red line plus/minus 95% confidence interval whiskers as a function of high ACE thresholds (abscissa), where the vertical dashed line indicates ACE = 245·10^4 kt^2 corresponding to the 2005 season. Horizontal colored bins show different PN categorizations according to the Intergovernmental Panel on Climate Change terminology.

from HighResMIP (see Materials and Methods) and compute the probability of necessary causation (PN) for different high ACE thresholds above the mean (Fig. 6C). If anthropogenic effects are a necessary condition for more active TC seasons, then PN > 0. Note that PN = 76% (likely; i.e., the intercept between the vertical dashed line and the red curve) for ACE = 245×10^4 kt^2 (i.e., a season similar to 2005). From Eq. 2, a PN = 76% (with a range of 50 to 89%) suggests that the probability of occurrence of a season similar to 2005 will increase around 4 times in the 2020 to 2049 period relative to the historical period (1970–2019). This suggests that anthropogenic effects will likely be a necessary condition for such an extreme ACE season to occur. Thus, we might expect extremely high TC activity (ACE > 210×10^4 kt^2; or when the red curve in Fig. 6C exceeds the probability $P = ⅔$, or above likely category, based on categorizations according to Intergovernmental Panel on Climate Change terminology) to become more common in the future under anthropogenic effects.

DISCUSSION

Most of the literature assesses the role of anthropogenic forcing from a mean activity change perspective (TC frequency, track, intensity, etc.). This work demonstrates that interannual variability changes have played a dominant role in determining the occurrence of both active and inactive TC seasons observed since around 1995. Also, increases in the mean and interannual variability have had a compounding (opposing) effect on the occurrence of active (inactive) TC seasons regarding ACE and TC count. It is also shown, using future projections from high-resolution HighResMIP model simulations and an ACE-proxy derived from CMIP6 models, that interannual variability of Atlantic TC activity is projected to increase as measured by ACE (36 ± 8%) and TC count (19 ± 11%). Both of these increases are significant relative to the variability of the historical period, and they will likely lead to more hyperactive hurricane seasons. In comparison, projected changes in the mean activity are much smaller with a projected mean ACE increase of 13 ± 8% and an insignificant 1 ± 3% change in mean TC number. These changes are the result of increased variability in TC relevant fields, such as vertical wind shear and atmospheric stability over the tropical North Atlantic basin in boreal summer, and are a response to enhanced interbasin Atlantic-Pacific SST variations. The enhanced future variability increase is near-homogeneously throughout the Atlantic basin. However, the mean changes show a dipole structure with an increased trend over the eastern and central Atlantic and a reduced trend over the Caribbean, which is similar to the observed trend (*12*). This suggests that the spatial inhomogeneities in TC activity trends cannot be attributed solely to observing system changes. Instead, changes in fundamental physical processes are underway due to anthropogenic effects, and these should be explored in future studies.

A future intensification in the variability of Atlantic TC activity would result in more extreme swings between active and inactive hurricane seasons, with important implications for seasonal outlooks. Enhanced variability is often associated with reduced prediction skill from enhanced weather noise (e.g., potential predictability, reduced signal-to-noise ratio, etc.). However, the projected increase in TC variance was shown here to be well explained by changes in known predictors (e.g., Niño 3-MDR interbasin SST index). This could lead to improved probabilistic seasonal outlooks for TC activity. In addition, intraseasonal variability associated with the "Madden-Julian oscillation is also projected to change in the future (*97*), which could have implications for subseasonal Atlantic TC activity. However, a comprehensive signal-to-noise analysis is required to separate the relative contributions of predicted versus unpredicted causes of enhanced TC variability, as well as their natural and/or external sources, such an analysis is beyond the scope of this work.

Last, the current NOAA/Climate Prediction Center seasonal outlooks for Atlantic TC activity rely on fixed thresholds for determining active (i.e., ACE > 130% of the 1951–2020 median; https://cpc.ncep.noaa.gov/products/outlooks/Background.html) and inactive seasons (i.e., ACE < 75% of the 1951–2020 median). Our results emphasize the need to reconcile the nonstationary behavior of the ACE PDF with current operational definitions of TC activity to account for the projected increase in extreme swings between active and inactive hurricane seasons.

MATERIALS AND METHODS

Observational data

TC data were obtained from the National Hurricane Center's second-generation hurricane database (HURDAT2) (*98*). To measure TC activity in the Atlantic basin, we use the ACE index (units of 10^4 kt^2), which is an integral measure of the number, strength, and duration of storms in a season (*99*). ACE is computed for each calendar year by summing the squared maximum wind velocity every 6 hours for each tropical and subtropical cyclone that is of tropical storm or hurricane strength (sustained winds greater than 34 kts). Out of season, TCs were included in the observed analysis; however, their contribution to seasonal ACE is minimal. Short-lived storms (<2 days) were excluded from the analysis as there has been a recent increase since around the year 2000, a fact that has been shown to be artificially created by the inhomogeneity in the observing systems and improvements in observational capabilities (*15*, *16*).

Observed SSTs are obtained from the Hadley Centre HadSSTv2 product at a 1° horizontal resolution for the period of 1900 to 2023 (*100*). Atmospheric variables (e.g., vertical profiles of temperature and winds) are obtained from monthly means of the European Center for Medium-Range Weather Forecast-5 Reanalysis (ERA5) (*101*) for the period of 1982 to 2023.

Model simulation—Direct TC detection from CMIP6 HighResMIP

Interannual variability of TC activity in climate models is diagnosed from direct simulations of TCs from the CMIP6 HighResMIP (see table S4 for list of models), which provides a multimodel, multiresolution ensemble protocol (*63*). The HighResMIPs are run under historical forcing for the period of 1950 to 2014 and future projections for the 2015 to 2050 with most of the forcing fields being the same as those used in the CMIP6 simulations (*102*). Aerosol properties are modeled by combining a climatological background natural aerosol with time-varying volcanic and time-varying anthropogenic aerosols from the Max Planck Institute Aerosol Climatology. These simulations only include interannual variations in volcanic and anthropogenic aerosols and exclude interannual variations in natural aerosols (*65*). For the future projections, greenhouse gases and aerosol concentrations from the high-end emission scenario of the Shared Socioeconomic Pathways (SSP585) were prescribed (*64*). The HighResMIP includes fully coupled and SST-prescribed runs. For the SST-prescribed runs, all

uncoupled models use the same observed SST and sea-ice forcing for the 1950 to 2014 period from the HadISST2 dataset at a 0.25° resolution. For the future projection period (2014–2050), the SST and sea-ice forcings are derived from the CMIP6 SSP585 greenhouse forcing simulations. The coupled models simulate their own SSTs (*65*).

TC detection in the HighResMIP

TCs are detected by two different tracking algorithms: TRACK (*103*) and TempestExtremes (*104*). The two tracking algorithms use different approaches; TRACK detects TCs by identifying vorticity features and accounting for warm core criteria, whereas TempestExtremes identifies TCs using sea-level pressure and warm-core criteria. Since the two trackers are fundamentally different (*68*), we use both to add confidence to the results. The increased horizontal resolution of the HighResMIP models has been shown to improve TC frequency and ACE representation in the North Atlantic, as well as the distribution of TC genesis, track, and intensity (*68*). The spatial pattern of TC transit per year is well represented, with spatial correlations $r > 0.9$ for both tracking algorithms; however, with considerably smaller amplitude than observed (figs. S7 and S8), the observed ACE-SST relationship is also well capture (fig. S3). Some of the deficiencies in representing TCs in HighResMIP include a lower TC frequency in the North Atlantic compared to observations, excessive TC activity in the Southern Hemisphere, and difficulty in simulating strong (categories 4 or 5) hurricanes (*68*). However, strong hurricane simulations are beyond the expected capabilities of these models (*105*).

Model simulations—Large scale analysis from CMIP6

Analysis of large-scale relevant fields for TC activity, such as vertical wind shear, humidity, and SST are taken from the CMIP6 model archive (https://esgf-node.llnl.gov/projects/cmip6/, see table S7 for list of models). The analysis comprises 15 CMIP6 models under historical radiative forcing (i.e., during 1920–2000). The future projection also comprises 15 CMIP6 models for the 2015 to 2100 period under the SSP585. Each model/ensemble member has a distinct climate trajectory due to differences in the atmospheric initial conditions. Differences among ensemble members from CMIP6 include interannual variability and model biases.

Interannual variability definition in observations and CMIP6 models

Interannual anomalies are defined by first subtracting the previous 30-year running mean climatology to remove trends due to anthropogenic effects. For example, the SST climatology for July 2000 is the averaged July SST from 1971 to 2000. This method defines anomalies relative to their contemporary climatology, and it is used at the National Oceanic and Atmospheric Administration's Climate Prediction Center to define anomalous climate events (e.g., ENSO). Since each CMIP6 model has its own physics and thus its own biases, we remove a 30-year running mean climatology derived for each CMIP6 model similar to what is done for the observational period. We tested the robustness of the 30-year running mean climatology by computing a new climatology at 5-year interval from 20- to 40-year running mean and the results are robust and independent of the choice of time window.

SGS distribution

Statistical modeling of TC-relevant fields using a SGS approach brings several benefits. First, it provides a method to quantify the influence of climate shifts under Gaussian and non-Gaussian assumptions. Second, it enables an investigation of how changes in the climate influence the statistical moments of TC-related variables and their PDFs, including the hypothesized increase in interannual variability due to enhanced ENSO and tropical North Atlantic SST variance. Changes in the PDF of TC activity (e.g., ACE, TC count) are modeled by an SGS distribution (*62*, *63*). The SGS distribution of a variable X is defined in Eq. 1, where E, g, b, and N are parameters obtained from the statistical moments of X following the method of moments (*62*).

$$\mathrm{SGS}(X) = \frac{1}{N}\left[(EX+g)^2 + b^2\right]^{-\left[1+\left(1/E^2\right)\right]} \exp\left[\frac{2g}{E^2 b}\left(\frac{EX+g}{b}\right)\right] \quad (1)$$

The SGS distribution accounts for non-Gaussian (i.e., nonzero skewness and kurtosis) characteristics of a variable, where the Gaussian distribution is a subset of the SGS distribution in the limit that parameter E approaches zero. For example, the PDFs of observed ACE and TC count are positively skewed, with heavier tails to the right of the mean (Fig. 1, E and F). Since the distribution parameters are a function of the statistical moments of variable X (*62*), then the sample variance, skewness, and kurtosis of a variable X are used to construct the SGS PDF. For example, to investigate changes in interannual variability only, the parameters of the SGS distributions are trained to account for changes in the variance while leaving all other statistical moments fixed. A goodness-of-fit analysis based on χ^2 and Kolmogorov-Smirnov tests show that the SGS is a good fit for the ACE and TC number data, whereas more traditional distributions (i.e., Poisson distributions) are not; this is because TC data are highly skewed and non-Gaussian (see table S2 and fig. S2 for details).

Attribution analysis

Causal counterfactual theory is used to assess the probability that an event E would not have occurred in the absence of a cause (C), where event E is defined as extremely active TC seasons measured by high ACE and C is ACC. A probability of necessary causation (PN) can be constructed to measure the fraction of extreme events attributed to ACC (*95*), defined as

$$\mathrm{PN}(C \rightarrow E) = \max\left\{1 - \frac{P_0}{P_1}, 0\right\} \quad (2)$$

where P_0 is the probability of an event occurring in the counterfactual world (i.e., without anthropogenic effects), and P_1 is the probability of that same event occurring in the factual world (i.e., with anthropogenic effects). P_0 and P_1 are obtained from the SGS PDF distribution (Eq. 1) applied to historical (1970–2019) and projected (2020–2049) TC activity, respectively, simulated by 87 HighResMIP models/ensembles. PN ranges from zero to one and indicates whether anthropogenic effects are a necessary condition for the extreme ACE to occur, i.e., whether the extreme event would occur in the absence of ACC.

Statistical significance test—Bootstrapping technique

A Monte Carlo bootstrapping method is used to determine confidence intervals by subsampling the dataset. All analyses presented are obtained by randomly selecting r samples out of n observations with replacement (Eq. 3). This is done 500 times to build a distribution of composites and assign 95th percentile confidence levels.

$$(n\ r) = \frac{n!}{r!(n-r)!} = \text{possible combinations} \quad (3)$$

Supplementary Materials

This PDF file includes:

Supplementary Text
Tables S1 to S7
Figs. S1 to S10
References

REFERENCES AND NOTES

1. M. J. Roberts, P. L. Vidale, M. S. Mizielinski, M.-E. Demory, R. Schiemann, J. Strachan, K. Hodges, R. Bell, J. Camp, Tropical cyclones in the UPSCALE ensemble of high-resolution global climate models. *J. Clim.* **28**, 574–596 (2015).
2. T. R. Knutson, J. J. Sirutis, M. Zhao, R. E. Tuleya, M. Bender, G. A. Vecchi, G. Villarini, D. Chavas, Global projections of intense tropical cyclone activity for the late twenty-first century from dynamical downscaling of CMIP5/RCP4.5 scenarios. *J. Clim.* **28**, 7203–7224 (2015).
3. H. Murakami, G. A. Vecchi, S. Underwood, T. L. Delworth, A. T. Wittenberg, W. G. Anderson, J.-H. Chen, R. G. Gudgel, L. M. Harris, S.-J. Lin, F. Zeng, Simulation and prediction of category 4 and 5 hurricanes in the high-resolution GFDL HiFLOR coupled climate model. *J. Clim.* **28**, 9058–9079 (2015).
4. M. F. Wehner, K. A. Reed, F. Li, J. Prabhat, C. T. Bacmeister, C.-T. Chen, C. Paciorek, P. J. Gleckler, K. R. Sperber, W. D. Collins, A. Gettelman, C. Jablonowski, The effect of horizontal resolution on simulation quality in the Community Atmospheric Model, CAM5.1. *J. Adv. Model. Earth Syst.* **6**, 980–997 (2014).
5. Y. Yamada, M. Satoh, M. Sugi, C. Kodama, A. T. Noda, M. Nakano, T. Nasuno, Response of tropical cyclone activity and structure to global warming in a high-resolution global nonhydrostatic model. *J. Clim.* **30**, 9703–9724 (2017).
6. T. R. Knutson, J. L. McBride, J. Chan, K. Emanuel, G. Holland, C. Landsea, I. Held, J. P. Kossin, A. K. Srivastava, M. Sugi, Tropical cyclones and climate change. *Nat. Geosci.* **3**, 157–163 (2010).
7. T. Knutson, S. J. Camargo, J. C. L. Chan, K. Emanuel, C.-H. Ho, J. Kossin, M. Mohapatra, M. Satoh, M. Sugi, K. Walsh, L. Wu, Tropical cyclones and climate change assessment: Part I: Detection and attribution. *Bull. Am. Meteorol. Soc.* **100**, 1987–2007 (2019).
8. S. I. Seneviratne, X. Zhang, M. Adnan, W. Badi, C. Dereczynski, A. Di Luca, S. Ghosh, I. Iskandar, J. Kossin, S. Lewis, F. Otto, I. Pinto, M. Satoh, S. M. Vicente-Serrano, M. Wehner, B. Zhou, R. Allan: "Weather and climate extreme events in a changing climate" in *Climate Change 2021: The Physical Science Basis. Contribution of Working Group I to the Sixth Assessment Report of the Intergovernmental Panel on Climate Change*, V. Masson-Delmotte, P. Zhai, A. Pirani, S. L. Connors, C. Péan, S. Berger, N. Caud, Y. Chen, L. Goldfarb, M. I. Gomis, M. Huang, K. Leitzell, E. Lonnoy, J. B. R. Matthews, T. K. Maycock, T. Waterfield, O. Yelekçi, R. Yu, B. Zhou, Eds. (Cambridge Univ. Press, Cambridge, United Kingdom and New York, NY, USA, 2021), pp. 1513–1766.
9. H. Murakami, T. L. Delworth, W. F. Cooke, M. Zhao, B. Xiang, P. C. Hsu, Detected climatic change in global distribution of tropical cyclones. *Proc. Natl. Acad. Sci. U.S.A.* **117**, 10706–10714 (2020).
10. P. J. Klotzbach, K. M. Wood, C. J. Schreck III, S. G. Bowen, C. M. Patricola, M. M. Bell, Trends in global tropical cyclone activity: 1990–2021. *Geophys. Res. Lett.* **49**, e2021GL095774 (2022).
11. H. Murakami, Substantial global influence of anthropogenic aerosols on tropical cyclones over the past 40 years. *Sci. Adv.* **8**, eabn9493 (2022).
12. G. A. Vecchi, T. R. Knutson, On estimates of historical North Atlantic tropical cyclone activity. *J. Clim.* **21**, 3580–3600 (2008).
13. P. J. Klotzbach, C. W. Landsea, Extremely intense hurricanes: Revisiting Webster et al. (2005) after 10 years. *J. Climate* **28**, 7621–7629 (2015).
14. J. R. Lanzante, Uncertainties in tropical-cyclone translation speed. *Nature* **570**, E6–E15 (2019).
15. C. W. Landsea, G. A. Vecchi, L. Bengtsson, T. R. Knutson, Impact of duration thresholds on Atlantic tropical cyclone counts. *J. Clim.* **23**, 2508–2519 (2010).
16. G. Villarini, G. A. Vecchi, T. R. Knutson, J. A. Smith, Is the recorded increase in short-duration North Atlantic tropical storms spurious? *J. Geophys. Res.* **116**, D10114 (2011).
17. X. Yan, R. Zhang, T. R. Knutson, The role of Atlantic overturning circulation in the recent decline of Atlantic major hurricane frequency. *Nat. Commun.* **8**, 1695 (2017).
18. S. B. Goldenberg, C. W. Landsea, A. M. Mestas-Nuñez, W. M. Gray, The recent increase in Atlantic hurricane activity: Causes and implications. *Science* **293**, 474–479 (2001).
19. W. Li, L. Li, Y. Deng, Impact of the interdecadal Pacific oscillation on tropical cyclone activity in the North Atlantic and eastern North Pacific. *Sci. Rep.* **5**, 12358 (2015).
20. J. Zhao, R. Zhan, Y. Wang, H. Xu, Contribution of the interdecadal Pacific oscillation to the recent abrupt decrease in tropical cyclone genesis frequency over the Western North Pacific since 1998. *J. Clim.* **31**, 8211–8224 (2018).
21. C. K. Folland, D. E. Parker, A. W. Colman, R. Washington, "Large scale modes of ocean surface temperature since the late nineteenth century," in *Beyond El Nino: Decadal and Interdecadal Climate Variability* (Springer, 1999), 73–102.
22. C. K. Folland, J. A. Renwick, M. J. Salinger, A. B. Mullan, Relative influences of the Interdecadal Pacific Oscillation and ENSO on the South Pacific Convergence Zone. *Geophys. Res. Lett.* **29**, 10.1029/2001GL014201 (2002).
23. T. Knutson, S. J. Camargo, J. C. L. Chan, K. Emanuel, C.-H. Ho, J. Kossin, M. Mohapatra, M. Satoh, M. Sugi, K. Walsh, L. Wu, Tropical cyclones and climate change assessment: Part II: Projected response to anthropogenic warming. *Bull. Am. Meteorol. Soc.* **101**, E303–E322 (2020).
24. S. B. Goldenberg, L. J. Shapiro, Physical mechanisms for the association of El Niño and west african rainfall with Atlantic major hurricane activity. *J. Climate* **9**, 1169–1187 (1996).
25. C. W. Landsea, A climatology of intense (or major) Atlantic hurricanes. *Mon. Weather Rev.* **121**, 1703–1713 (1993).
26. C. W. Landsea, G. D. Bell, W. M. Gray, S. B. Goldenberg, The extremely active 1995 Atlantic hurricane season: Environmental conditions and verification of seasonal forecasts. *Mon. Weather Rev.* **126**, 1174–1193 (1998).
27. G. J. Alaka Jr., E. D. Maloney, The influence of the MJO on upstream precursors to African easterly waves. *J. Clim.* **25**, 3219–3236 (2012).
28. P. J. Klotzbach, E. C. J. Oliver, Modulation of Atlantic basin tropical cyclone activity by the Madden–Julian oscillation (MJO) from 1905 to 2011. *J. Clim.* **28**, 204–217 (2015).
29. G. R. Foltz, M. J. McPhaden, R. Lumpkin, A strong Atlantic Meridional Mode event in 2009: The role of mixed layer dynamics. *J. Clim.* **25**, 363–380 (2012).
30. L. Jiang, T. Li, Relative roles of El Niño-induced extratropical and tropical forcing in generating Tropical North Atlantic (TNA) SST anomaly. *Clim. Dyn.* **53**, 3791–3804 (2019).
31. J.-H. Park, T. Li, Interdecadal modulation of El Niño–tropical North Atlantic teleconnection by the Atlantic multi-decadal oscillation. *Clim. Dyn.* **52**, 5345–5360 (2019).
32. S.-P. Xie, S. G. H. Philander, A coupled ocean-atmosphere model of relevance to the ITCZ in the eastern Pacific. *Tellus A* **46**, 340–350 (1994).
33. L. Xie, T. Yan, L. J. Pietrafesa, J. M. Morrison, T. Karl, Climatology and interannual variability of North Atlantic hurricane tracks. *J. Climate* **18**, 5370–5381 (2005).
34. D. J. Vimont, J. P. Kossin, The Atlantic meridional mode and hurricane activity. *Geophys. Res. Lett.* **34**, L07709 (2007).
35. D. B. Enfield, D. A. Mayer, Tropical Atlantic sea surface temperature variability and its relation to El Niño-Southern Oscillation. *J. Geophys. Res.* **102**, 929–945 (1997).
36. S.-K. Lee, D. B. Enfield, C. Wang, Why do some El Niños have no impact on tropical North Atlantic SST? *Geophys. Res. Lett.* **35**, L16705 (2008).
37. J. C. H. Chiang, Y. Kushnir, A. Giannini, Deconstructing Atlantic Intertropical Convergence Zone variability: Influence of the local cross-equatorial sea surface temperature gradient and remote forcing from the eastern equatorial Pacific. *J. Geophys. Res. Atmos.* **107**, 10.1029/2000JD000307 (2002).
38. D. J. Amaya, M. J. DeFlorio, A. J. Miller, S.-P. Xie, WES feedback and the Atlantic Meridional Mode: Observations and CMIP5 comparisons. *Clim. Dyn.* **49**, 1665–1679 (2017).
39. Y. Yang, S.-P. Xie, L. Wu, Y. Kosaka, J. Li, ENSO forced and local variability of North Tropical Atlantic SST: Model simulations and biases. *Clim. Dyn.* **51**, 4511–4524 (2018).
40. J. C. H. Chiang, A. H. Sobel, Tropical tropospheric temperature variations caused by ENSO and their influence on the remote tropical climate. *J. Clim.* **15**, 2616–2631 (2002).
41. W. M. Gray, Atlantic seasonal hurricane frequency. Part I: El Niño and 30 mb quasi-biennial oscillation influences. *Mon. Weather Rev.* **112**, 1649–1668 (1984).
42. L. J. Shapiro, Month-to-month variability of the Atlantic tropical circulation and its relationship to tropical storm formation. *Mon. Weather Rev.* **115**, 2598–2614 (1987).
43. J. P. Kossin, S. J. Camargo, M. Sitkowski, Climate modulation of North Atlantic hurricane tracks. *J. Climate* **23**, 3057–3076 (2010).
44. P. J. Klotzbach, El Niño–Southern Oscillation's impact on Atlantic basin hurricanes and U.S. Landfalls. *J. Clim.* **24**, 1252–1263 (2011).
45. S. Larson, S. Lee, C. Wang, E. Chung, D. Enfield, Impacts of non-canonical El Niño patterns on Atlantic hurricane activity. *Geophys. Res. Lett.* **39**, L14706 (2012).
46. J. P. Kossin, D. J. Vimont, A more general framework for understanding Atlantic hurricane variability and trends. *Bull. Amer. Meteor. Soc.* **88**, 1767–1782 (2007).
47. M. Latif, N. Keenlyside, J. Bader, Tropical sea surface temperature, vertical wind shear, and hurricane development. *Geophys. Res. Lett.* **34**, L01710 (2007).
48. S.-K. Lee, D. B. Enfield, C. Wang, Future impact of differential interbasin ocean warming on Atlantic hurricanes. *J. Clim.* **24**, 1264–1275 (2011).
49. K. L. Swanson, Nonlocality of Atlantic tropical cyclone intensities. *Geochem. Geophys. Geosyst.* **9**, Q04V01 (2008).
50. C. Wang, S.-K. Lee, Global warming and United States landfalling hurricanes. *Geophys. Res. Lett.* **35**, L02708 (2008).
51. R. West, H. Lopez, S. Lee, A. E. Mercer, D. Kim, G. R. Foltz, K. Balaguru, Seasonality of interbasin SST contributions to Atlantic tropical cyclone activity. *Geophys. Res. Lett.* **49**, e2021GL096712 (2022).
52. S. J. Camargo, M. Ting, Y. Kushnir, Influence of local and remote SST on North Atlantic tropical cyclone potential intensity. *Clim. Dyn.* **40**, 1515–1529 (2013).
53. P. J. Klotzbach, The influence of El Niño–Southern Oscillation and the Atlantic multidecadal oscillation on caribbean tropical cyclone Activity. *J. Clim.* **24**, 721–731 (2011).

54. C. M. Patricola, R. Saravanan, P. Chang, The impact of the El Niño–Southern Oscillation and Atlantic meridional mode on seasonal Atlantic tropical cyclone activity. *J. Clim.* **27**, 5311–5328 (2014).
55. H. Lopez, S.-K. Lee, D. Kim, A. T. Wittenberg, S.-W. Yeh, Projections of faster onset and slower decay of El Niño in the 21st century. *Nat. Commun.* **13**, 1915 (2022).
56. Y. Yang, L. Wu, Y. Guo, B. Gan, W. Cai, G. Huang, X. Li, T. Geng, Z. Jing, S. Li, X. Liang, S.-P. Xie, Greenhouse warming intensifies north tropical Atlantic climate variability. *Sci. Adv.* **7**, eabg9690 (2021).
57. W. Cai, A. Santoso, G. Wang, S.-W. Yeh, S.-I. An, K. M. Cobb, M. Collins, E. Guilyardi, F.-F. Jin, J.-S. Kug, M. Lengaigne, M. J. McPhaden, K. Takahashi, A. Timmermann, G. Vecchi, M. Watanabe, L. Wu, ENSO and greenhouse warming. *Nat. Clim. Change* **5**, 849–859 (2015).
58. H. A. Rashid, A. C. Hirst, S. J. Marsland, An atmospheric mechanism for ENSO amplitude changes under an abrupt quadrupling of CO_2 concentration in CMIP5 models. *Geophys. Res. Lett.* **43**, 1687–1694 (2016).
59. A. C. T. Sena, C. M. Patricola, B. Loring, Future changes in active and inactive Atlantic hurricane seasons in the energy exascale earth system model. *Geophys. Res. Lett.* **49**, e2022GL100267 (2022).
60. E. K. M. Chang, Y. Guo, Is the number of North Atlantic tropical cyclones significantly underestimated prior to the availability of satellite observations? *Geophys. Res. Lett.* **34**, L14801 (2007).
61. H. Murakami, T. Li, P.-C. Hsu, Contributing factors to the recent high level of Accumulated Cyclone Energy (ACE) and Power Dissipation Index (PDI) in the North Atlantic. *J. Clim.* **27**, 3023–3034 (2014).
62. P. D. Sardeshmukh, G. P. Compo, C. Penland, Need for caution in interpreting extreme weather statistics. *J. Clim.* **28**, 9166–9187 (2015).
63. P. D. Sardeshmukh, P. Sura, Reconciling non-Gaussian climate statistics with linear dynamics. *J. Clim.* **22**, 1193–1207 (2009).
64. R. J. Haarsma, M. J. Roberts, P. L. Vidale, C. A. Senior, A. Bellucci, Q. Bao, P. Chang, S. Corti, N. S. Fučkar, V. Guemas, J. von Hardenberg, W. Hazeleger, C. Kodama, T. Koenigk, L. R. Leung, J. Lu, J.-J. Luo, J. Mao, M. S. Mizielinski, R. Mizuta, P. Nobre, M. Satoh, E. Scoccimarro, T. Semmler, J. Small, J.-S. von Storch, High Resolution Model Intercomparison Project (HighResMIP v1.0) for CMIP6. *Geosci. Model Dev.* **9**, 4185–4208 (2016).
65. M. J. Roberts, J. Camp, J. Seddon, P. L. Vidale, K. Hodges, B. Vannière, J. Mecking, R. Haarsma, A. Bellucci, E. Scoccimarro, L.-P. Caron, F. Chauvin, L. Terray, S. Valcke, M.-P. Moine, D. Putrasahan, C. D. Roberts, R. Senan, C. Zarzycki, P. Ullrich, Y. Yamada, R. Mizuta, C. Kodama, D. Fu, Q. Zhang, G. Danabasoglu, N. Rosenbloom, H. Wang, L. Wu, Projected future changes in tropical cyclones using the CMIP6 HighResMIP multimodel ensemble. *Geophys. Res. Lett.* **47**, e2020GL088662 (2020).
66. A. Bellucci, S. Gualdi, A. Navarra, The double-ITCZ syndrome in coupled general circulation models: The role of large-scale vertical circulation regimes. *J. Clim.* **23**, 1127–1145 (2010).
67. A. A. Scaife, D. Copsey, C. Gordon, C. Harris, T. Hinton, S. Keeley, A. O'Neill, M. Roberts, K. Williams, Improved Atlantic winter blocking in a climate model. *Geophys. Res. Lett.* **38**, L23703 (2011).
68. M. J. Roberts, J. Camp, J. Seddon, P. L. Vidale, K. Hodges, B. Vanniere, J. Mecking, R. Haarsma, A. Bellucci, E. Scoccimarro, L.-P. Caron, F. Chauvin, L. Terray, S. Valcke, M.-P. Moine, D. Putrasahan, C. Roberts, R. Senan, C. Zarzycki, P. Ullrich, Impact of model resolution on tropical cyclone simulation using the HighResMIP–PRIMAVERA multimodel *Ensemble*. *J. Clim.* **33**, 2557–2583 (2020).
69. G. Villarini, G. A. Vecchi, Projected increases in North Atlantic tropical cyclone intensity from CMIP5 models. *J. Clim.* **26**, 3231–3240 (2013).
70. E. Scoccimarro, A. Bellucci, A. Storto, S. Gualdi, S. Masina, A. Navarra, "Remote subsurface ocean temperature as a predictor of Atlantic hurricane activity," in *Proceedings of the National Academy of Sciences* (National Academy of Sciences, 2018), pp. 11460–11464.
71. K. Hu, G. Huang, P. Huang, Y. Kosaka, S.-P. Xie, Intensification of El Niño-induced atmospheric anomalies under greenhouse warming. *Nat. Geosci.* **14**, 377–382 (2021).
72. G. J. Holland, Misuse of landfall as a proxy for Atlantic tropical cyclone activity. *EOS Trans. Am. Geophys. Union* **88**, 349–350 (2007).
73. R. Seager, N. Henderson, M. Cane, Persistent discrepancies between observed and modeled trends in the tropical Pacific Ocean. *J. Climate* **35**, 4571–4584 (2022).
74. A. J. Colbert, B. J. Soden, Climatological variations in North Atlantic tropical cyclone tracks. *J. Clim.* **25**, 657–673 (2012).
75. M. Liu, G. A. Vecchi, J. A. Smith, H. Murakami, The present-day simulation and twenty-first-century projection of the climatology of extratropical transition in the North Atlantic. *J. Clim.* **30**, 2739–2756 (2017).
76. H. Murakami, B. Wang, Future change of North Atlantic tropical cyclone tracks: Projection by a 20-km-mesh global atmospheric model. *J. Clim.* **23**, 2699–2721 (2010).
77. K. Yoshida, M. Sugi, R. Mizuta, H. Murakami, M. Ishii, Future changes in tropical cyclone activity in high-resolution large-ensemble simulations. *Geophys. Res. Lett.* **44**, 9910–9917 (2017).
78. D. Kim, S.-K. Lee, H. Lopez, G. R. Foltz, C. Wen, R. West, J. Dunion, Increase in Cape Verde hurricanes during Atlantic Niño. *Nat. Commun.* **14**, 3704 (2023).
79. G. A. Vecchi, B. J. Soden, A. T. Wittenberg, I. M. Held, A. Leetmaa, M. J. Harrison, Weakening of tropical Pacific atmospheric circulation due to anthropogenic forcing. *Nature* **441**, 73–76 (2006).
80. I. M. Held, B. J. Soden, Robust responses of the hydrological cycle to global warming. *J. Clim.* **19**, 5686–5699 (2006).
81. G. A. Meehl, W. M. Washington, El Niño-like climate change in a model with increased atmospheric CO_2 concentrations. *Nature* **382**, 56–60 (1996).
82. P. N. DiNezio, A. C. Clement, G. A. Vecchi, B. J. Soden, B. P. Kirtman, S.-K. Lee, Climate response of the equatorial Pacific to global warming. *J. Clim.* **22**, 4873–4892 (2009).
83. G. A. Vecchi, B. J. Soden, Effect of remote sea surface temperature change on tropical cyclone potential intensity. *Nature* **450**, 1066–1070 (2007).
84. M. DeMaria, J. Kaplan, An updated statistical hurricane intensity prediction scheme (SHIPS) for the Atlantic and eastern North Pacific basins. *Weather Forecast.* **14**, 326–337 (1999).
85. R. Klaver, R. Haarsma, P. L. Vidale, W. Hazeleger, Effective resolution in high resolution global atmospheric models for climate studies. *Atmos. Sci. Lett.* **21**, e952 (2020).
86. H. J. Diamond, C. J. Schreck, A. Allgood, E. J. Becker, E. S. Blake, F. G. Bringas, S. J. Camargo, R. Cerveny, L. Chen, C. A. S. Coelho, H. J. Diamond, C. Earl-Spurr, N. Fauchereau, C. Fogarty, S. B. Goldenberg, D. S. Harnos, Q. He, Z.-Z. Hu, P. J. Klotzbach, J. A. Knaff, A. Kumar, M. L'Heureux, C. W. Landsea, I.-I. Lin, H. Lopez, A. M. Lorrey, J.-J. Luo, A. D. Magee, R. J. Pasch, L. Paterson, A. B. Pezza, M. Rosencrans, C. J. Schreck, B. C. Trewin, R. E. Truchelut, J. Uehling, B. Wang, H. Wang, K. M. Wood, The tropics. *Bull. Am. Meteorol. Soc.* **105**, S214–S276 (2024).
87. K. Emanuel, S. Solomon, D. Folini, S. Davis, C. Cagnazzo, Influence of tropical tropopause layer cooling on Atlantic hurricane activity. *J. Clim.* **26**, 2288–2301 (2013).
88. A. A. Wing, K. Emanuel, S. Solomon, On the factors affecting trends and variability in tropical cyclone potential intensity. *Geophys. Res. Lett.* **42**, 8669–8677 (2015).
89. J. P. Kossin, Validating atmospheric reanalysis data using tropical cyclones as thermometers. *Bull. Am. Meteorol. Soc.* **96**, 1089–1096 (2015).
90. R. Knutti, R. Furrer, C. Tebaldi, J. Cermak, G. A. Meehl, Challenges in combining projections from multiple climate models. *J. Clim.* **23**, 2739–2758 (2010).
91. R. T. Sutton, G. D. McCarthy, J. Robson, B. Sinha, A. T. Archibald, L. J. Gray, Atlantic Multidecadal Variability and the U.K. ACSIS Program. *Bull. Am. Meteorol. Soc.* **99**, 415–425 (2018).
92. R. Zhang, On the persistence and coherence of subpolar sea surface temperature and salinity anomalies associated with the Atlantic multidecadal variability. *Geophys. Res. Lett.* **44**, 7865–7875 (2017).
93. B. B. B. Booth, N. J. Dunstone, P. R. Halloran, T. Andrews, N. Bellouin, Aerosols implicated as a prime driver of twentieth-century North Atlantic climate variability. *Nature* **484**, 228–232 (2012).
94. A. Bellucci, A. Mariotti, S. Gualdi, The role of forcings in the twentieth-century North Atlantic multidecadal variability: The 1940–75 North Atlantic cooling case study. *J. Clim.* **30**, 7317–7337 (2017).
95. J. Pearl, *Casuality: Models, Reasoning and Inference* (Cambridge Univ. Press, 2000).
96. A. Hannart, P. Naveau, Probabilities of causation of climate changes. *J. Clim.* **31**, 5507–5524 (2018).
97. C.-W. J. Chang, W.-L. Tseng, H.-H. Hsu, N. Keenlyside, B.-J. Tsuang, The Madden-Julian Oscillation in a warmer world. *Geophys. Res. Lett.* **42**, 6034–6042 (2015).
98. C. W. Landsea, J. L. Franklin, Atlantic hurricane database uncertainty and presentation of a new database format. *Mon. Weather Rev.* **141**, 3576–3592 (2013).
99. G. D. Bell, M. S. Halpert, R. C. Schnell, R. W. Higgins, J. Lawrimore, V. E. Kousky, R. Tinker, W. Thiaw, M. Chelliah, A. Artusa, Climate assessment for 1999. *Bull. Am. Meteorol. Soc.* **81**, s1–s50 (2000).
100. N. A. Rayner, D. E. Parker, E. B. Horton, C. K. Folland, L. V. Alexander, D. P. Rowell, E. C. Kent, A. Kaplan, Global analyses of sea surface temperature, sea ice, and night marine air temperature since the late nineteenth century. *J. Geophys. Res. Atmos.* **108**, 4407 (2003).
101. H. Hersbach, B. Bell, P. Berrisford, S. Hirahara, A. Horányi, J. Muñoz-Sabater, J. Nicolas, C. Peubey, R. Radu, D. Schepers, A. Simmons, C. Soci, S. Abdalla, X. Abellan, G. Balsamo, P. Bechtold, G. Biavati, J. Bidlot, M. Bonavita, G. De Chiara, P. Dahlgren, D. Dee, M. Diamantakis, R. Dragani, J. Flemming, R. Forbes, M. Fuentes, A. Geer, L. Haimberger, S. Healy, R. J. Hogan, E. Hólm, M. Janisková, S. Keeley, P. Laloyaux, P. Lopez, C. Lupu, G. Radnoti, P. de Rosnay, I. Rozum, F. Vamborg, S. Villaume, J. Thépaut, The ERA5 global reanalysis. *Q. J. R. Meteorol. Soc.* **146**, 1999–2049 (2020).
102. V. Eyring, S. Bony, G. A. Meehl, C. A. Senior, B. Stevens, R. J. Stouffer, K. E. Taylor, Overview of the Coupled Model Intercomparison Project Phase 6 (CMIP6) experimental design and organization. *Geosci. Model Dev.* **9**, 1937–1958 (2016).
103. K. Hodges, A. Cobb, P. L. Vidale, How well are tropical cyclones represented in reanalysis datasets? *J. Clim.* **30**, 5243–5264 (2017).

104. P. A. Ullrich, C. M. Zarzycki, TempestExtremes: A framework for scale-insensitive pointwise feature tracking on unstructured grids. *Geosci. Model Dev.* **10**, 1069–1090 (2017).
105. C. A. Davis, Resolving tropical cyclone intensity in models. *Geophys. Res. Lett.* **45**, 2082–2087 (2018).
106. A. Cherchi, P. G. Fogli, T. Lovato, D. Peano, D. Iovino, S. Gualdi, S. Masina, E. Scoccimarro, S. Materia, A. Bellucci, A. Navarra, Global mean climate and main patterns of variability in the CMCC-CM2 coupled model. *J. Adv. Model. Earth Syst.* **11**, 185–209 (2019).
107. R. Haarsma, M. Acosta, R. Bakhshi, P.-A. B. Bretonnière, L.-P. Caron, M. Castrillo, S. Corti, P. Davini, E. Exarchou, F. Fabiano, U. Fladrich, R. F. Franco, J. García-Serrano, J. von Hardenberg, T. Koenigk, X. Levine, V. Meccia, T. van Noije, G. van den Oord, F. M. Palmeiro, M. Rodrigo, Y. Ruprich-Robert, P. Le Sager, É. Tourigny, S. Wang, M. van Weele, K. Wyser, HighResMIP versions of EC-Earth: EC-Earth3P and EC-Earth3P-HR. Description, model performance, data handling and validation. *Geosci. Model Dev.* **13**, 3507–3527 (2020).
108. M. J. Roberts, A. Baker, E. W. Blockley, D. Calvert, A. Coward, H. T. Hewitt, L. C. Jackson, T. Kuhlbrodt, P. Mathiot, C. D. Roberts, R. Schiemann, J. Seddon, B. Vannière, P. L. Vidale, Description of the resolution hierarchy of the global coupled HadGEM3-GC3.1 model as used in CMIP6 HighResMIP experiments. *Geosci. Model Dev.* **12**, 4999–5028 (2019).
109. A. Voldoire, CNRM-CERFACS CNRM-CM6-1 model output prepared for CMIP6 HighResMIP, version 20230220, Earth System Grid Federation (2019); https://doi.org/10.22033/ESGF/CMIP6.1925.
110. J.-S. von Storch, D. Putrasahan, K. Lohmann, O. Gutjahr, J. Jungclaus, M. Bittner, H. Haak, K.-H. Wieners, M. Giorgetta, C. Reick, M. Esch, V. Gayler, P. de Vrese, T. Raddatz, T. Mauritsen, J. Behrens, V. Brovkin, M. Claussen, T. Crueger, I. Fast, S. Fiedler, S. Hagemann, C. Hohenegger, T. Jahns, S. Kloster, S. Kinne, G. Lasslop, L. Kornblueh, J. Marotzke, D. Matei, K. Meraner, U. Mikolajewicz, K. Modali, W. Müller, J. Nabel, D. Notz, K. Peters-von Gehlen, R. Pincus, H. Pohlmann, J. Pongratz, S. Rast, H. Schmidt, R. Schnur, U. Schulzweida, K. Six, B. Stevens, A. Voigt, E. Roeckner, MPI-M MPIESM1.2-HR model output prepared for CMIP6 HighResMIP, version 20230720, Earth System Grid Federation (2017); https://doi.org/10.22033/ESGF/CMIP6.762.
111. H.-M. Kim, M.-I. Lee, P. J. Webster, D. Kim, J. H. Yoo, A physical basis for the probabilistic prediction of the accumulated tropical cyclone kinetic energy in the Western North Pacific. *J. Clim.* **26**, 7981–7991 (2013).
112. X. Wang, Y. Han, W. Xue, G. Yang, G. J. Zhang, Stable climate simulations using a realistic general circulation model with neural network parameterizations for atmospheric moist physics and radiation processes. *Geosci. Model Dev.* **15**, 3923–3940 (2022).

Acknowledgments: We thank the anonymous reviewers whose comments improved the manuscript. **Funding:** This research was carried out in part under the auspices of the Cooperative Institute for Marine and Atmospheric Studies, a cooperative institute of the University of Miami and the NOAA, cooperative agreement NA 20OAR4320472. H.L. acknowledges support from NOAA/CPO/MAPP Award NA19OAR4310282. **Author contributions:** H.L. conceived the study and wrote the initial draft of the paper. H.L., S.-K.L., R.W., D.K., G.R.F., G.J.A., and H.M. contributed to the design, the statistical analysis, and interpretation of the results, as well as the writing of the final version of the paper. **Competing interests:** The authors declare that they have no competing interests. **Data and materials availability:** All data used in this study are available online. The Atlantic hurricane database (HURDAT2) from 1851 to 2023 is freely available at https://nhc.noaa.gov/data/. Hadley Centre Sea Ice and Sea Surface Temperature (HadSST) data were downloaded from Met Office Hadley Centre at https://metoffice.gov.uk/hadobs/hadisst/. The ERA5 data were downloaded from ECMWF at https://ecmwf.int/en/forecasts/dataset/ecmwf-reanalysis-v5. HighResMIP and CMIP6 model archive data are freely available at: https://esgf-node.llnl.gov/projects/cmip6/. All statistical analyses were performed using the Grid Analysis and Display System (GrADS), which are publicly available from the Center for Ocean-Land-Atmosphere Studies at http://cola.gmu.edu/grads and NCL, which is publicly available from the NCAR Command Language (NCL) at https://www.ncl.ucar.edu/. All data needed to evaluate the conclusions in the paper are present in the paper and/or the Supplementary Materials.

Submitted 30 May 2024
Accepted 16 October 2024
Published 15 November 2024
10.1126/sciadv.adq7856